

Self-assembling peptide gels promote angiogenesis and functional recovery after spinal cord injury in rats

Journal of Tissue Engineering
Volume 13: 1–14
© The Author(s) 2022
Article reuse guidelines:
sagepub.com/journals-permissions
DOI: 10.1177/20417314221086491
journals.sagepub.com/home/tej



Jin Young Hong^{1,2*}, Su Hee Kim^{3,4*}, Yoojin Seo³,
Jooik Jeon^{1,2} , Ganchimeg Davaa^{1,2}, Jung Keun Hyun^{1,2,7} 
and Soo Hyun Kim^{3,5,6}

Abstract

Spinal cord injury (SCI) leads to disruption of the blood–spinal cord barrier, hemorrhage, and tissue edema, which impair blood circulation and induce ischemia. Angiogenesis after SCI is an important step in the repair of damaged tissues, and the extent of angiogenesis strongly correlates with the neural regeneration. Various biomaterials have been developed to promote angiogenesis signaling pathways, and angiogenic self-assembling peptides are useful for producing diverse supramolecular structures with tunable functionality. RADA16 (Ac-RARADADARARADADA-NH₂), which forms nanofiber networks under physiological conditions, is a self-assembling peptide that can provide mechanical support for tissue regeneration and reportedly has diverse roles in wound healing. In this study, we applied an injectable form of RADA16 with or without the neuropeptide substance P to the contused spinal cords of rats and examined angiogenesis within the damaged spinal cord and subsequent functional improvement. Histological and immunohistochemical analyses revealed that the inflammatory cell population in the lesion cavity was decreased, the vessel number and density around the damaged spinal cord were increased, and the levels of neurofilaments within the lesion cavity were increased in SCI rats that received RADA16 and RADA16 with substance P (rats in the RADA16/SP group). Moreover, real-time PCR analysis of damaged spinal cord tissues showed that IL-10 expression was increased and that locomotor function (as assessed by the Basso, Beattie, and Bresnahan (BBB) scale and the horizontal ladder test) was significantly improved in the RADA16/SP group compared to the control group. Our findings indicate that RADA16 modified with substance P effectively stimulates angiogenesis within the damaged spinal cord and is a candidate agent for promoting functional recovery post-SCI.

Keywords

Spinal cord injury, self-assembling peptide, substance P, angiogenesis, functional recovery

Date received: 29 November 2021; accepted: 23 February 2022

¹Department of Nanobiomedical Science and BK21 NBM Global Research Center for Regenerative Medicine, Dankook University, Cheonan, Republic of Korea

²Institute of Tissue Regeneration Engineering, Dankook University, Cheonan, Republic of Korea

³Center for Biomaterials, Biomedical Research Institute, Korea Institute of Science and Technology, Seoul, Republic of Korea

⁴Medifab Ltd., Seoul, Republic of Korea

⁵Korea Institute of Science and Technology Europe, Saarbrücken, Germany

⁶NBIT, KU-KIST Graduate School of Converging Science and Technology, Korea University, Seoul, Republic of Korea

⁷Department of Rehabilitation Medicine, College of Medicine, Dankook University, Cheonan, Republic of Korea

*These authors have contributed equally to this work.

Corresponding authors:

Jung Keun Hyun, Department of Rehabilitation Medicine, College of Medicine, Dankook University, 119 Dandae-ro, Anseo-dong, Dongnam-gu, Cheonan 31116, Republic of Korea.

Email: rhhyun@dankook.ac.kr

Soo Hyun Kim, Korea Institute of Science and Technology Europe, Campus E7 1, 66123 Saarbrücken, Germany.

Email: soohkim@kist.re.kr



Introduction

Spinal cord injury (SCI), which causes trauma in most cases, leads to complex pathophysiological changes, including inflammation, axonal injury and demyelination, cystic cavitation, glial scar formation, neuronal cell death, oxidative stress, and vascular disruption or ischemia.^{1,2} Angiogenesis is an important factor that facilitates neuronal regeneration after SCI.³ In previous studies, biomaterials,^{4–6} stem cells,⁷ exosomes from neural stem cells,^{8,9} or extracorporeal shock waves¹⁰ were used to enhance vessel formation and were found to result in functional recovery in *in vivo* SCI models.

RADA16 (Ac-RARADADARARADADA-NH₂) is a common self-assembling peptide that forms nanofiber networks under physiological conditions.¹¹ It is used as an extracellular matrix that provides mechanical support for wound healing and tissue regeneration and can also be used as a hemostatic agent in the clinical setting.¹² In recent studies on spinal cord regeneration, microvascular cells or neural stem/progenitor cells were transplanted with RADA16 into the contused spinal cords of rats, and RADA16 was found to attenuate inflammation and glial scar formation by inducing the neural differentiation of transplanted stem cells.^{13,14} Modification of RADA16 with proangiogenic peptides, such as SVVYGLR derived from osteopontin, might enhance angiogenesis after central nervous system (CNS) lesions.¹⁵ Notably, in our previous works, RADA16 modified with substance P showed a good therapeutic effect on hindlimb ischemia and promoted skin regeneration by acting as a good delivery system and recruiting intrinsic mesenchymal stem cells in various tissue defect models.^{16,17} Substance P, a small 11-amino-acid endogenous neuropeptide, is known to have an important role in cell proliferation, bone marrow fibrosis, and the regulation of wound healing, and it is an injury-inducible factor that acts to induce mobilization of CD29+ stromal-like cells in wound-healing processes.¹⁸ The release of substance P induces the recruitment of circulating cells with angiogenic activity from the blood to the injury site, resulting in enhanced angiogenesis,¹⁹ and substance P is also useful for the treatment of cardiovascular disease and limb ischemia.¹⁸ Therefore, long-term delivery of substance P leads to efficient induction of key cells for tissue regeneration, maximizing the regeneration effect. Herein, we applied RADA16 modified with substance P to a rat spinal cord contusion injury model, hypothesizing that it might exert proangiogenic effects in addition to the other effects of RADA16 and might consequently aid functional recovery after SCI.

Materials and methods

Peptide synthesis and preparation

The peptides RADA16 (Ac-RARADADARARADADA-NH₂) and RADA16-SP (Ac-RARADADARARADAD

AGGRPKPQQFFGLM-NH₂) were synthesized (Peptron, Daejeon, Korea). In RADA16-SP, RADA16 and substance P are linearly bound via two glycine linkers. That is, one molecule of substance P is bound to each molecule of RADA16, and 1 μ L of RADA16-SP contains 5 μ g of substance P. The peptides were dissolved in a 295 nM sucrose solution to prepare a 1% (w/v) peptide hydrogel. RADA16 and RADA16-SP were mixed at different concentrations and administered to different experimental groups. The experimental groups were as follows: (1) the phosphate-buffered saline (PBS) group; (2) RADA16 group; and (3) RADA16 + RADA16-SP (RADA16/SP) group. RADA16 and RADA16-SP were mixed at a ratio of 7:3 (v/v). The total amount of substance P in the samples was 15 μ g. Then, the peptide hydrogel was sonicated with an ultrasonic cleanser for 30 min as previously described.²⁰ For *in vitro* gelation, RADA16 and RADA16-SP were mixed with DPBS containing calcium and magnesium and gelled immediately after mixing.

Structural characterization

The structures of the peptide gels were examined by transmission electron microscopy (TEM). The samples were diluted in distilled water to a working concentration of 0.01% and stained with 2% uranyl acetate. To determine the structures of the peptide gels, circular dichroism (CD) spectra of the peptide gels were obtained using a spectropolarimeter (JASCO, Inc.). RADA16, RADA16-SP, and RADA16/SP were prepared by diluting the peptide solutions in distilled water to working concentrations of 0.02% (wt/vol) and then incubating them at room temperature overnight. For CD spectra measurements, samples were added to a quartz cuvette with a 1-mm path length (Hellma Standard Cuvette 110QS (Quartz Suprasil); Hellma Analytics).²¹

Rheological studies

The viscoelastic properties of the self-assembling peptides were measured by a rotational rheometer (MCR302, Anton Paar, Austria). Samples were analyzed after gelation of RADA16 and RADA16 + RADA16-SP (RADA16/SP). The angular frequency was in the range of 0.5–20, and the experiment was conducted at room temperature.

Cell culture and live/dead assay

Primary cortical neurons were prepared from Sprague-Dawley rat embryos (embryonic day 16) as described previously. Briefly, each embryo was placed in Hank's balanced salt solution (HBSS; Gibco BRL, Grand Island, NY, USA). The embryos were decapitated at the head/neck junction using small surgical scissors, and the meninges covering each brain hemisphere were manually peeled off

using #5 fine forceps. The cortex was washed twice with HBSS and then transferred to a 15-mL conical tube containing 2 mL of 2.5 mg/mL papain solution (Sigma-Aldrich, St. Louis, MO, USA) in HBSS. After 15 min of incubation at 37°C, the supernatant was discarded, and the cells were washed twice in 2 mL of HBSS and then centrifuged for 3 min. The cell pellet was resuspended in 1 mL of neurobasal medium (Gibco, Waltham, MA, USA) supplemented with B27 (Invitrogen Life Technologies, Carlsbad, CA, USA), GlutaMAX (Invitrogen Life Technologies), and 1% penicillin/streptomycin (Gibco) by gentle trituration with a 1-mL pipet tip. Single cells were mixed with the peptide gels without bubbling. Then, the cells were plated on 18-mm circular coverslips (Paul Marienfeld GmbH & Co., Lauda-Königshofen, Germany) and incubated in 5% CO₂ at 37°C for 3 days.

Cell viability was determined by the live/dead cell assay (Molecular Probes, Eugene, OR, USA) according to the manufacturer's instructions. In brief, staining solution containing 2 mM calcein AM and 4 mM ethidium homodimer-1 (EthD-1) in Dulbecco's phosphate-buffered saline (DPBS) was prepared. Calcein AM was used to label live cells green, while EthD-1 stained dead cells red. The culture medium was discarded, and each sample was incubated in 100 µL of staining solution for 45 min at room temperature. For the quantification of cell viability, six randomized images from each group were captured at 40× magnification via confocal microscopy (LSM 700; Carl Zeiss, Oberkochen, Germany). Live cells were quantified by counting the number of green cells using the cell counter plug-in of ImageJ software (1.37V, National Institutes of Health, Bethesda, MD). Cell viability is expressed as a percentage of live cells relative to the total number of cells as previously described.²²

Spinal cord contusion injury model and treatments

Female Sprague–Dawley rats (12 weeks old, 230–250 g) were used for the experiments. All animal experiments were approved by the Institutional Animal Care and Use Committee of Dankook University (approval no. 19-010). The animals were housed individually in an environment at a constant temperature (23°C–25°C) and humidity (45%–50%) with free access to food and water under specific pathogen-free (SPF) conditions. The surgical procedures have been previously described in detail.²³ Briefly, rats were anesthetized by inhalation of 3% isoflurane (Forane; Choongwae Pharma, Seoul, Korea), and a laminectomy was performed at the T9 level. The exposed spinal cord was moderately contused with an Infinite Horizon impactor (IH-400, Precision Systems and Instrumentation). Thirty minutes after the injury, 10 µL of RADA16 ($n=10$) or RADA16/SP ($n=9$) was injected into the epicenter of the lesion site at a rate of 1 µL/min. The same amount of PBS was injected into the control group ($n=10$). After

injection, the injured spinal cord was covered with homeostatic material (Surgicel fabric, Johnson and Johnson, Arlington, TX), and the skin was sutured in layers. All rats that underwent surgery were injected with 40 mg/kg cefotiam hydrochloride (Fontiam™, Hanmi Pharma, Seoul, Korea) intramuscularly for 3 days and were injected with normal saline (3 mL) intraperitoneally after the surgery. The animals also received oral administration of 10 mg/kg acetaminophen syrup (Tylenol™, Janssen Pharmaceutica, Titusville, NJ) for 3 days, and bladder expression was performed twice a day until the amount of expressed urine was less than 0.5 mL/day.

Histology

All rats were sacrificed and perfused with 0.9% normal saline and 4% paraformaldehyde (PFA) by cardiac perfusion at 8 weeks for histological or molecular biology analysis. The extracted spinal cords were postfixed in 4% PFA for 24 h and cryoprotected in 30% sucrose for 3 days. Spinal cords were embedded in M1 compound (Thermo Fisher Scientific, Waltham, Massachusetts, USA) and cryosectioned sagittally to a thickness of 16 µm. The sectioned tissues were stained with hematoxylin and eosin (H&E) to confirm the cavity size. Briefly, the sections were rinsed in PBS and then put into H&E solutions. After washing with tap water for 2 min, the sections were dehydrated through a graded ethanol series, cleared with xylene and imaged using a Nikon microscope. The area of the lesion cavity was determined by sagittal H&E images taken from the lesion epicenter ($n=4$ per group). The lesion cavity was outlined manually in each image, and its area was analyzed using ImageJ software (National Institutes of Health) as previously described.²²

Immunohistochemistry

Tissue sections were stained for inflammation and angiogenesis markers using antibodies against ED1 (1:1000; Abcam plc, Cambridge, MA, USA), GFAP (1:1000; DAKO, Carpinteria, CA, USA), CD31 (1:200; Santa Cruz, CA, USA), and VEGF (1:200; Santa Cruz). The sections were treated for 5 min in 0.2% Triton X-100, washed three times in PBS for 5 min, and then blocked in 2% normal goat serum for 1 h at room temperature. Then, they were incubated with primary antibodies overnight at 4°C in 2% goat serum. After washing with PBS, the sections were incubated with goat anti-rabbit (1:200; Jackson ImmunoResearch) and goat anti-mouse (1:200; Jackson ImmunoResearch) secondary antibodies diluted in 2% normal goat serum for 2 h. Following incubation, the sections were washed three times for 5 min with PBS and mounted with fluorescence mounting medium (DAKO Cytomation). Images were acquired using a confocal microscope (LSM 700; Carl Zeiss). The inflammatory response was analyzed by manually counting the total number of ED1+ cells within the lesion cavity. In addition, the

Table 1. Primer sequences used for gene expression analysis by real-time PCR.

Gene	Forward (5'–3')	Reverse
IL-1 β	CACCTTCTTTTCCTTCATCTTTG	GTCGTTGCTTGCTCTCCTTGT
IL-6	ACCACCCACAACAGACCAGT	CAGAATTGCCATTGCACAAC
TNF- α	CCCTGGTACTAACTCCCAGAAA	TGTATGAGAGGGACGGAACC
IL-10	CAGCTGCGACGCTGTCATCG	CAGCTGCGACGCTGTCATCG
Caspase 3	GCATTCCCATAAGCCTCCT	TTGTCACATGGGAACACATTTT
VWF	CAATTCTCGGAACTTCCAA	GGCAAACAAATGGATGTCAA
18S rRNA	CATTCGAACGTCTGCCCTAT	GTTTCTCAGGCTCCCTCTCC

CD31- and VEGF-stained areas were quantified with the vessel analysis plug-in of ImageJ software using the following three parameters (five independent areas, $n=4$ per group): (1) average vessel diameter (μm); (2) vessel density/field (%); and (3) number of vessels/field.

3-3'-Diaminobenzidine tetrahydrochloride (DAB) staining was performed using a neurofilament 200 kDa (NF200) antibody (Millipore, Billerica, MA, USA) to confirm axon regeneration. Sections were incubated in 0.3% H_2O_2 for 30 min at room temperature to inactivate endogenous peroxidase activity, incubated with 0.2% Triton X-100 for 5 min, and blocked with 10% normal goat serum for 1 h. The NF200 antibody was diluted 1:200 in 2% BSA/PBS and incubated overnight at 4°C. After overnight incubation, the sections were washed three times for 5 min each in 0.1M PBS. The sections were incubated with biotinylated secondary antibodies (1:200, Jackson Immunoresearch Laboratories, West Grove, PA) for 2 h at room temperature and then washed three times. The signals were enhanced with the Vectastain ABC kit (Vector Laboratories, Burlingame, CA, USA) for 30 min. The antigen-antibody complexes were then visualized with 0.05% DAB (Sigma) solution/0.06% NiCl_2 (Sigma) solution containing 0.003% H_2O_2 , and the reaction was stopped with distilled water. The sections were dehydrated in a graded ethanol series, cleared with xylene, and mounted with p-xylene-bis-pyridinium bromide (DPX) (Sigma). Images were captured by a Nikon microscope. Axons labeled with NF200 in the lesion cavity were quantified using ImageJ software (National Institutes of Health) as described in a previous study.²² Briefly, the number of pixels occupied by NF200-labeled axons in each image ($n=4$ per group) taken with a Nikon microscope with a 20 \times objective lens was quantified and divided by the total number of pixels in the field to obtain the mean axon density per field. This value is expressed as a percentage.

Real-time PCR

To confirm the changes in the expression levels of proinflammatory and anti-inflammatory genes (tumor necrosis factor alpha (TNF- α), interleukin (IL)-6, IL-1 beta

(IL-1 β), caspase 3, and IL-10) and angiogenesis-related genes (von Willebrand factor (vWF)) in each group, RNA levels in spinal cord tissues were analyzed using real-time PCR. In brief, spinal cord samples were homogenized with a Taco™ prep bead beater system (Taco, Taichung, Taiwan), and total RNA was isolated using an RNeasy mini kit (Qiagen, Hilden, Germany). cDNA was synthesized using random hexamer primers and SuperScript IV reverse transcriptase (Invitrogen Life Technologies). All primer pairs were designed using UCSC Genome Bioinformatics and the NCBI database, and their sequences are listed in Table 1. Real-time PCR was performed using Fast SYBR Green Master Mix (Applied Biosystems, Foster City, CA, USA) on a StepOne Real-Time PCR system (Applied Biosystems). Each reaction was performed at least in triplicate. The expression of each target gene was normalized to the expression of 18S rRNA and is expressed as the fold change relative to that in the control group.

Functional analysis

We evaluated the degree of functional recovery after SCI using two methods: the Basso, Beattie, and Bresnahan (BBB) scale and the horizontal ladder test. The BBB scale, which includes scores ranging from 0 to 21 (0=no hindlimb movement, 21=normal hindlimb movement), was used to assess hindlimb locomotor function.²⁴ The score was determined by two observers who were blinded to the treatment groups. The rats were positioned across from each observer, and both sides of the rats were observed during 4 min of walking in an open field arena (cylindrical-shaped acrylic box; 90 cm diameter, 15 cm high) with a smooth floor. The horizontal ladder test was performed using a runway with acrylic walls (10 cm tall, 127 cm long, 8 cm wide between walls, 1 cm between rungs).²² All rats were trained to walk on a horizontal ladder before the test. Testing was started 1 week after SCI and continued weekly. Rats that exhibited hindlimb weight support (BBB score greater than 10) were made to walk across the horizontal ladder three times, and the number of footfalls for each hindpaw was analyzed and calculated as described below.²²

$$\text{Ladder score} = \frac{\text{erroneous steps involving the hindpaw}}{\text{total steps involving the hindpaw}} \times 100 (\%)$$

The functional analysis was performed by a blinded investigator until the end of the study.

Statistical analysis

All numeric data are reported as the means \pm standard deviations (SDs), and IBM SPSS Statistics 26 (International Business Machines Corp., Armonk, NY, USA) was used for the analysis. The Shapiro–Wilk test was performed to confirm the normal distribution of all quantitative histological and functional data from each group, and according to the results, parametric or nonparametric tests were chosen. The Mann–Whitney U test was performed to analyze the differences between rheological data for RADA16 and RADA16/SP. For histological, immunohistochemical and quantitative PCR data, one-way analysis of variance (ANOVA), and the Games–Howell post hoc test were used to analyze differences among the control, RADA16 and RADA16/SP groups. Repeated measures two-way ANOVA (time and group) was used to compare locomotor function parameters, including BBB scores and performance on the ladder test, among the control and experimental groups, and then the Bonferroni post hoc test was used to analyze data from each time point. $p < 0.05$ was considered significant.

Results

Characteristics of RADA16 and RADA16/SP

The nanostructures of the peptide hydrogels were observed by TEM. The results confirmed that RADA16 was composed of ~5–10-nm nanofibers, but RADA16-SP had more of a random structure and did not form nanofibers (Figure 1(c) and (d)). Figure 1(e) shows that the structure of RADA16 + RADA16-SP (RADA16/SP) is mostly similar to that of RADA16. To determine the secondary structures of the peptide hydrogels, the CD spectra of RADA16, RADA16-SP, and RADA16/SP were analyzed. If a peptide formed a β -sheet structure, it showed a positive peak in the range of 195–216 nm. According to the results (Figure 1), RADA16 and RADA16/SP showed a peak in this range, whereas RADA16-SP did not. RADA16-SP flowed when the plate was tilted 45° after gelation, while RADA16 and RADA16/SP retained their shape.

The rheological characteristics of the peptides before and after gelation were analyzed. The storage modulus values of RADA16 and RADA16/SP after gelation increased approximately 3.77 times and 2.88 times, respectively, compared to the values before gelation. On the other hand, RADA16-SP had similar storage modulus values before and after gelation. Although RADA16-SP did

not gel alone, it was confirmed that the material mixed with RADA16 improved the physical properties of the hydrogel through the gelation of RADA16 (Figure 1(g)). Additionally, the complex viscosity values of RADA16 and RADA16/SP were 58.42 ± 3.99 – 26.86 ± 1.03 Pa/s, respectively, at 0.5 rad/s (Figure 1(h)). These results confirmed that the complex viscosity of RADA16/SP was approximately 46% of that of RADA16.

We examined the effects of encapsulation by the peptide hydrogels on cell viability. Our results showed that the percentages of cells encapsulated cells positive for calcein-AM (green) in RADA16 or RADA16/SP were similar to that in the control group (Figure 2(a)–(c)). The relative percentage of viable cells was not significantly different between the RADA16 and RADA16/SP groups and the control group and was nearly maintained at 100% (Figure 2(d)).

RADA16/SP reduced the inflammatory cell population in the lesion cavity but did not reduce the cavity area in the spinal cord

To examine the effects of RADA16 and RADA16/SP on the inflammatory response after SCI, 8 weeks after treatment, we evaluated the size of the lesion cavity in H&E-stained tissue sections (Figure 3(a)). In all groups, cavities with areas ranging from 3 to 5 mm² were formed in the injured spinal cord. The cavity size was the largest in the RADA16 group, with a maximum of approximately 5 mm², due to the injected hydrogel remaining in the lesion site. There was no significant difference between the control and experimental groups with respect to the cavity area (Figure 3(b)). However, the number of ED1+ active microglia/macrophages infiltrating the injury site was significantly decreased in the RADA16/SP group compared to the control group (Figure 3(c) and (d)).

We further analyzed the angiogenic effect of RADA16 and RADA16/SP after SCI. Immunohistochemical analysis of CD31 was performed 8 weeks postimplantation (Figure 4(a), (c) and (e)). The mean vessel diameter in the lesion site was not significantly different between the groups (Figure 4(g)), but the density and number of vessels were significantly increased in the RADA16/SP group compared to the control group (Figure 4(h) and (i)). To analyze the proangiogenic signal, we examined VEGF expression in the implanted spinal cord by immunohistochemistry (Figure 4(b), (d) and (f)). There were no significant differences in the mean VEGF+ vessel diameter in the lesion epicenter between the groups (Figure 4(j)), but the VEGF+ vessel density and number in the lesion epicenter were significantly higher in the RADA16/SP group than in the control group (Figure 4(k) and (l)).

Furthermore, we evaluated the effects of RADA16 and RADA16/SP on axonal regrowth after SCI. Tissue was stained with an antibody against the protein neurofilament

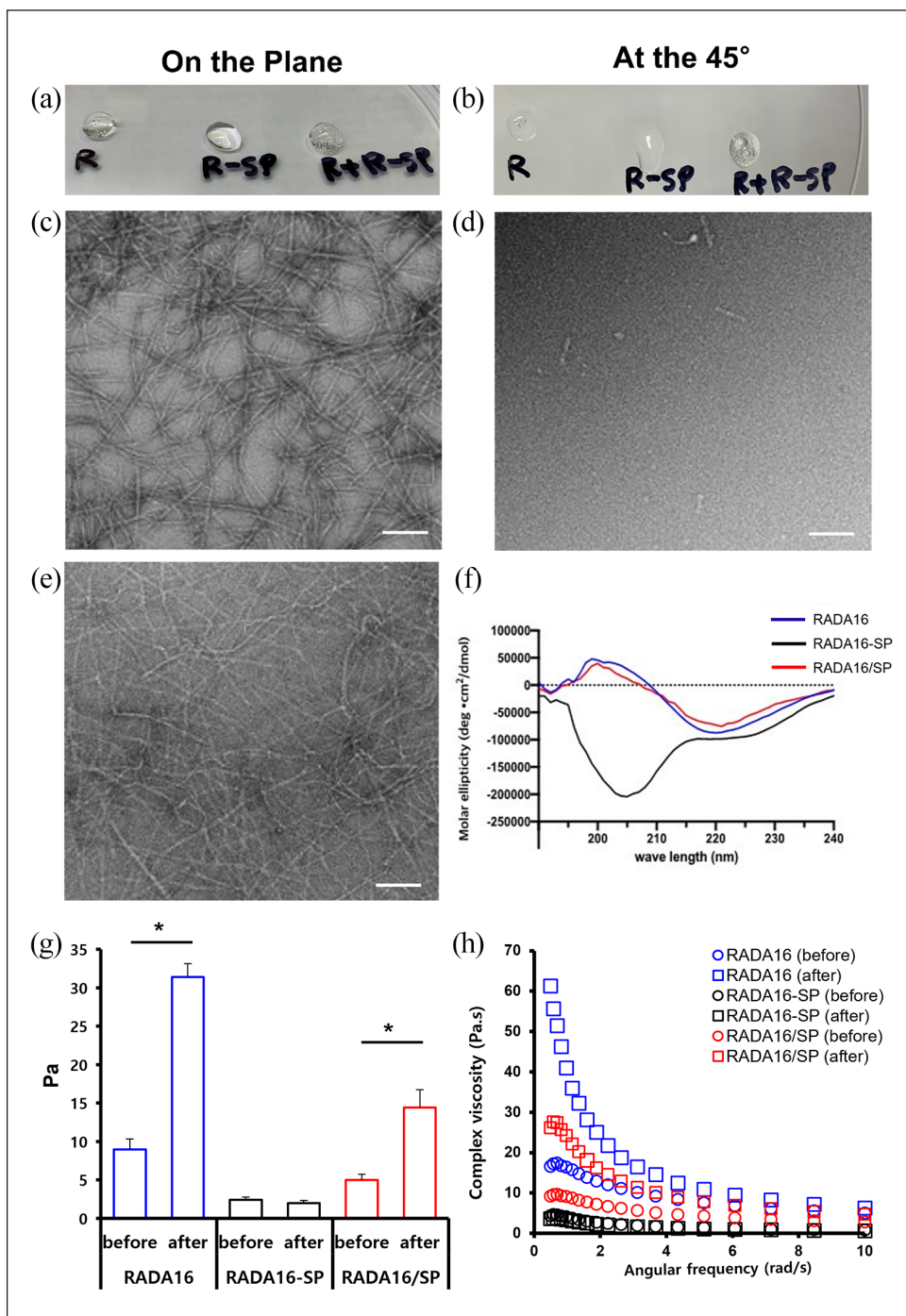


Figure 1. Structural and rheological characterization of bioactive peptide gels. Optical examination of the peptides RADA16 (R), RADA16-SP (R-SP), and RADA + RADA16-SP (R + R-SP) on the horizontal plane (a) and a 45° inclined plane (b). EM images of the peptides RADA16 (c), RADA16-SP (d), and RADA16/SP (RADA16 + RADA16-SP) (e). White scale bar = 100 μm . (f) CD of RADA16 (blue), RADA16-SP (black), and RADA16/SP (red). (g) Storage modulus and (h) complex viscosity of RADA16 (blue), RADA16-SP (black), and RADA16/SP (red) before and after gelation. * $p < 0.05$, the Mann–Whitney U test.

200 kDa (NF200) using DAB (Figure 5(a)–(c)). The implanted hydrogel was slightly biodegraded after 8 weeks, but most of it remained in the injection site. We examined the NF200+ axons that had regenerated into the hydrogel (Figure 5(b) and (c)). Quantitative analyses showed that

the NF200+ axon density was significantly increased in the RADA16/SP group compared with the control group (Figure 5(d)). The number of NF200+ axons was also significantly increased in the RADA16/SP group compared with the control group (Figure 5(e)). The number of

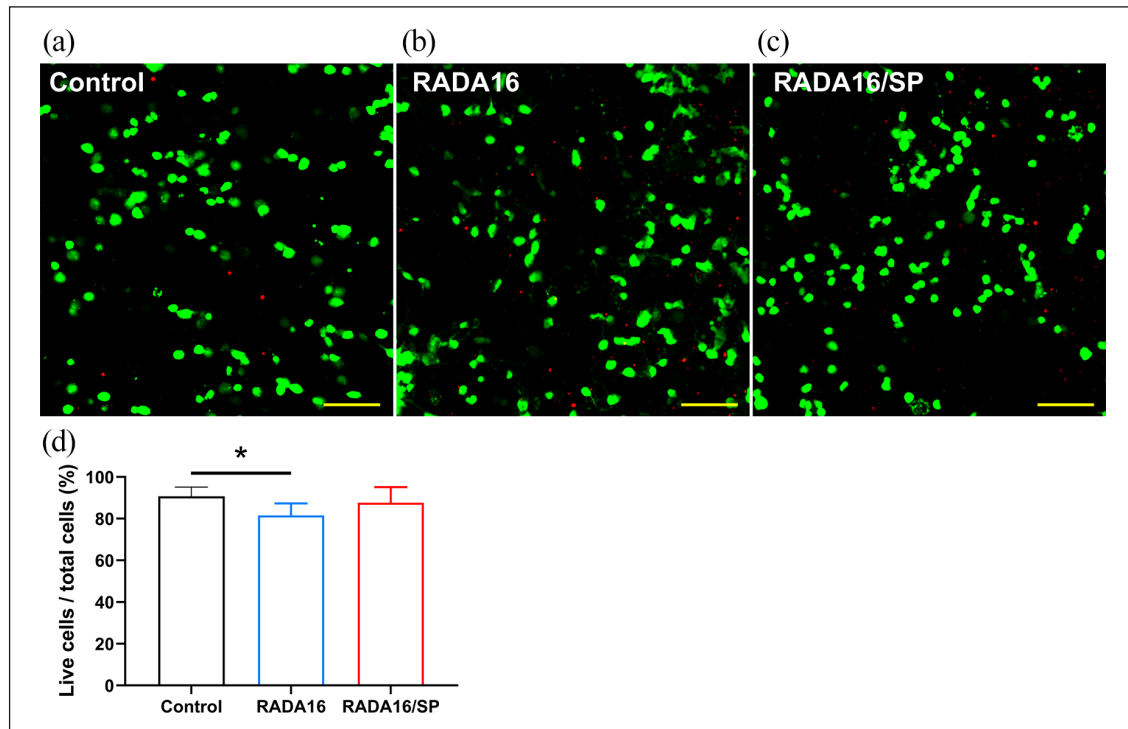


Figure 2. Representative images of live and dead staining of cortical neurons in the collagen (a), RADA16 (b) and RADA16/SP (c) groups on day 3 and the ratio of live cells to total stained cells ($n=4$ per group) (d). Yellow scale bar = $50\ \mu\text{m}$. * $p < 0.05$, one-way ANOVA followed by the Games-Howell post hoc test.

NF200+ axons was significantly increased in the RADA16 group, and the ratio of NF200+ axons to total axons was even higher in the RADA16/SP group. These findings demonstrate that RADA16/SP improves angiogenesis and axonal regeneration after SCI.

RADA16/SP altered inflammation- and angiogenesis-related gene expression

Furthermore, we assessed changes in the expression levels of genes involved in inflammation and angiogenesis in the spinal cord through real-time PCR (Figure 6). The mRNA levels of TNF- α , which is a representative proinflammatory cytokine, were significantly increased in the RADA16/SP group compared with the control group (Figure 6(a)). However, the levels of other inflammatory cytokines, namely, IL-6, IL-1 β , and caspase 3, showed no significant difference between the RADA16/SP and control groups, and the IL-1 β expression level was significantly increased in the RADA16 group compared to the control group (Figure 6(b)–(d)). The levels of representative anti-inflammatory cytokines, particularly IL-10, were higher in the RADA16/SP group compared with the control group (Figure 6(e)). We further analyzed the expression levels of genes associated with angiogenesis after injection of RADA16 or RADA16/SP hydrogel into SCI rats. Our data showed that the expression level of vWF, a major gene

involved in the angiogenesis process, was significantly increased in the RADA16/SP group compared to the control (Figure 6(f)).

RADA16/SP improved the locomotor performance of SCI rats

We used the BBB scale, and the horizontal ladder test to assess functional recovery 8 weeks after injury. According to BBB scores, functional recovery was significantly higher in the RADA16/SP group than in the control group 5 weeks after SCI (Figure 7(a)). The number of missed steps in the horizontal ladder test was significantly lower in the RADA16/SP group than in the control group from 5 weeks after SCI until sacrifice (Figure 7(b)). These results confirm that RADA16/SP improves locomotor function after SCI.

Discussion

One of the promising strategies in the field of tissue regeneration is the utilization of endogenous wound-healing mechanisms. Self-assembling peptides have several advantages for tissue regeneration and wound healing, such as biomimetic tunability, a low immune response, and the ability to easily be combined various cytokines or cells.^{12,25} The RADA16 peptide, which has the sequence

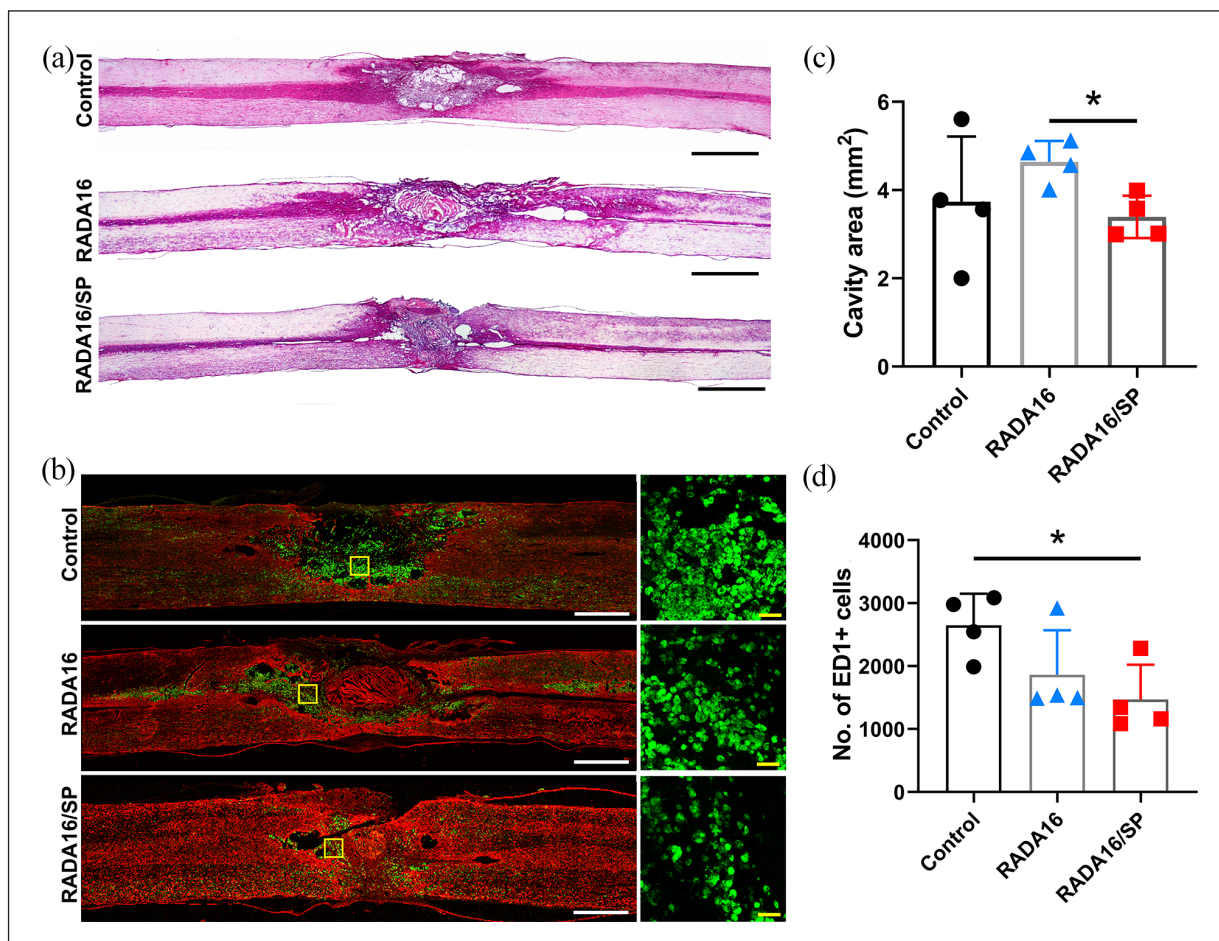


Figure 3. Representative images of H&E staining (a) and immunohistochemistry (b) for ED1 (green) and GFAP (red) in the injured spinal cord 8 weeks after injection of control, RADA16 or RADA16/SP. For low magnification images, a 10 \times objective was used; white scale bar, 1 mm. The yellow boxes are magnified on the right side; yellow scale bar, 50 μ m. The cavity of the lesion was measured from sagittal H&E staining images ($n=4$ per group) (c), and the total number of ED1 + inflammatory cells was counted within the lesion epicenter (1 mm²) ($n=4$ per group) (d). The data are expressed as the mean \pm SD. * $p < 0.05$, one-way ANOVA followed by the Games-Howell post hoc test.

Ac-RARADADARARADADA-NH₂, consists of alternating hydrophilic residues and hydrophobic residues. This oligopeptide forms stable β -sheets in the presence of salt ions and is short and simple; thus, it can be self-assembled through weak interactions such as hydrogen bonds, ionic bonds, hydrophobic interactions, and van der Waals interactions. Through such structural changes, RADA16 peptides become nanofibers.²⁶ RADA16-SP consists of 29 amino acids, and since substance P is not an alternating sequence and is relatively long, it may interfere with intermolecular interactions. This leads to random structuring of the peptide,²⁰ whose spectrum is quite different from that of RADA16 (Figure 1(f)). Therefore, in this study, we mixed RADA16-SP with RADA16 at a vol% ratio of 3:7 and obtained very stable β -sheet structures with similar CD spectra (Figure 1(f)). It is important to achieve sufficient blood flow to the injury site by forming stable, mature vessel networks for tissue regeneration; therefore,

long-term delivery of angiogenic factors is necessary. Substance P conjugated to RADA16 is retained in the body longer than soluble substance P, which plays a critical role in forming mature vessels. In our previous work, RADA16-SP was more effective than soluble substance P in delivering substance P to the injury region. The substance P moiety in RADA16 \pm RADA16-SP was observed to be present in the body for up to 28 days and was able to help form mature vessels, confirming that it improved tissue regeneration.^{20,21} In addition, since the mechanical properties of RADA16 and RADA16 + RADA16-SP might be different, it cannot be excluded that these differences substantially affected the histological and functional results.

In this study, we found that the numbers of ED1 + macrophages and microglia in the lesioned spinal cord were decreased after the application of the mixture of RADA16 and RADA16-SP but that the numbers of macrophages

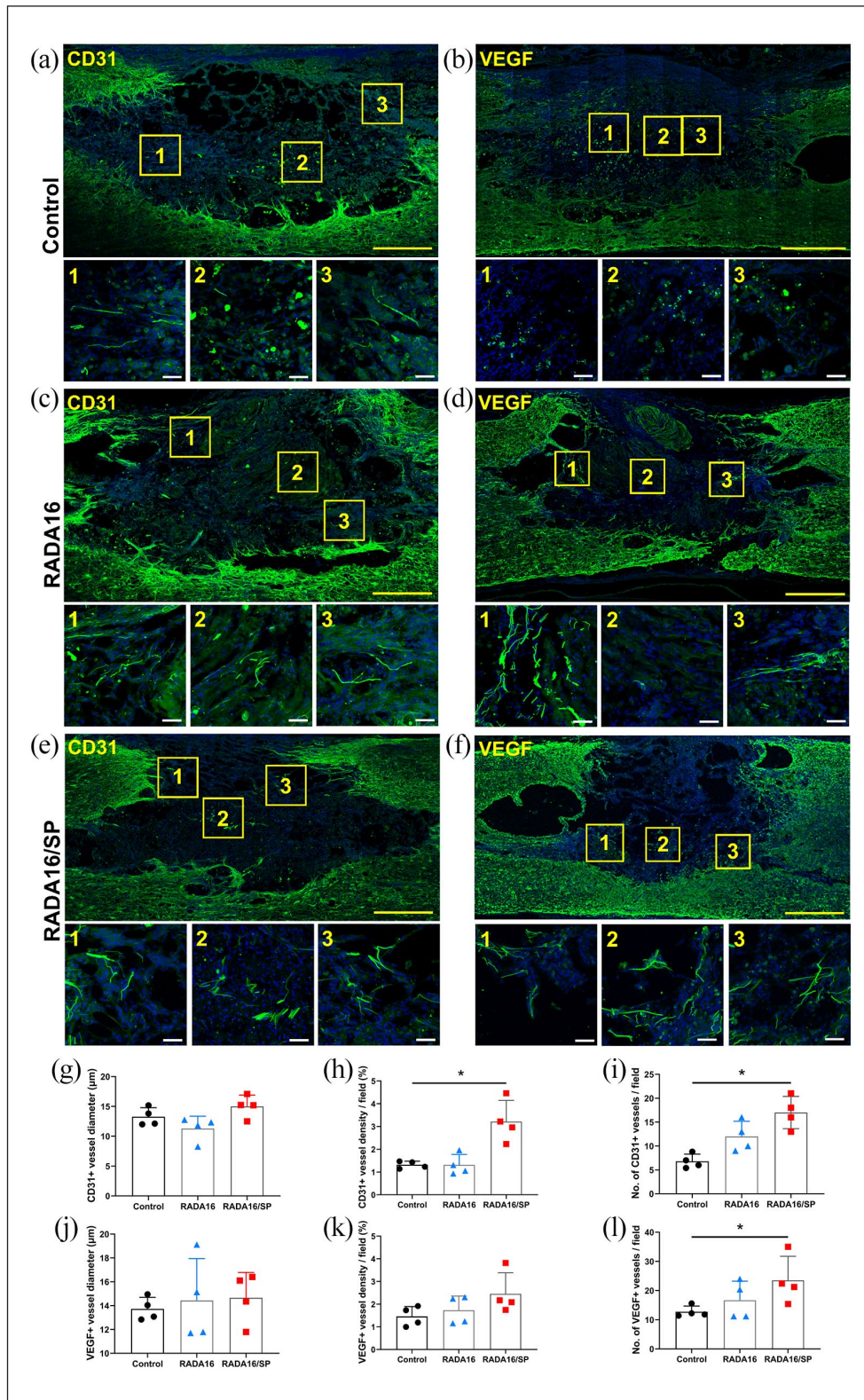


Figure 4. Spinal cord tissues immunostained with CD31 and VEGF antibodies and with DAPI from the control (a and b), RADA16 (c and d), and RADA16/SP (e and f) groups 8 weeks after injection. A 20× objective was used to obtain these images; yellow scale bar, 500 µm. The yellow boxes are magnified on the right side; white scale bar, 50 µm. The mean diameter (g and j), density (h and k), and number per field (i and l) of CD31+ or VEGF+ vessels within the lesion epicenter were quantified in 3 20× fields (n=4 per group). *p < 0.05, one-way ANOVA followed by the Games-Howell post hoc test.

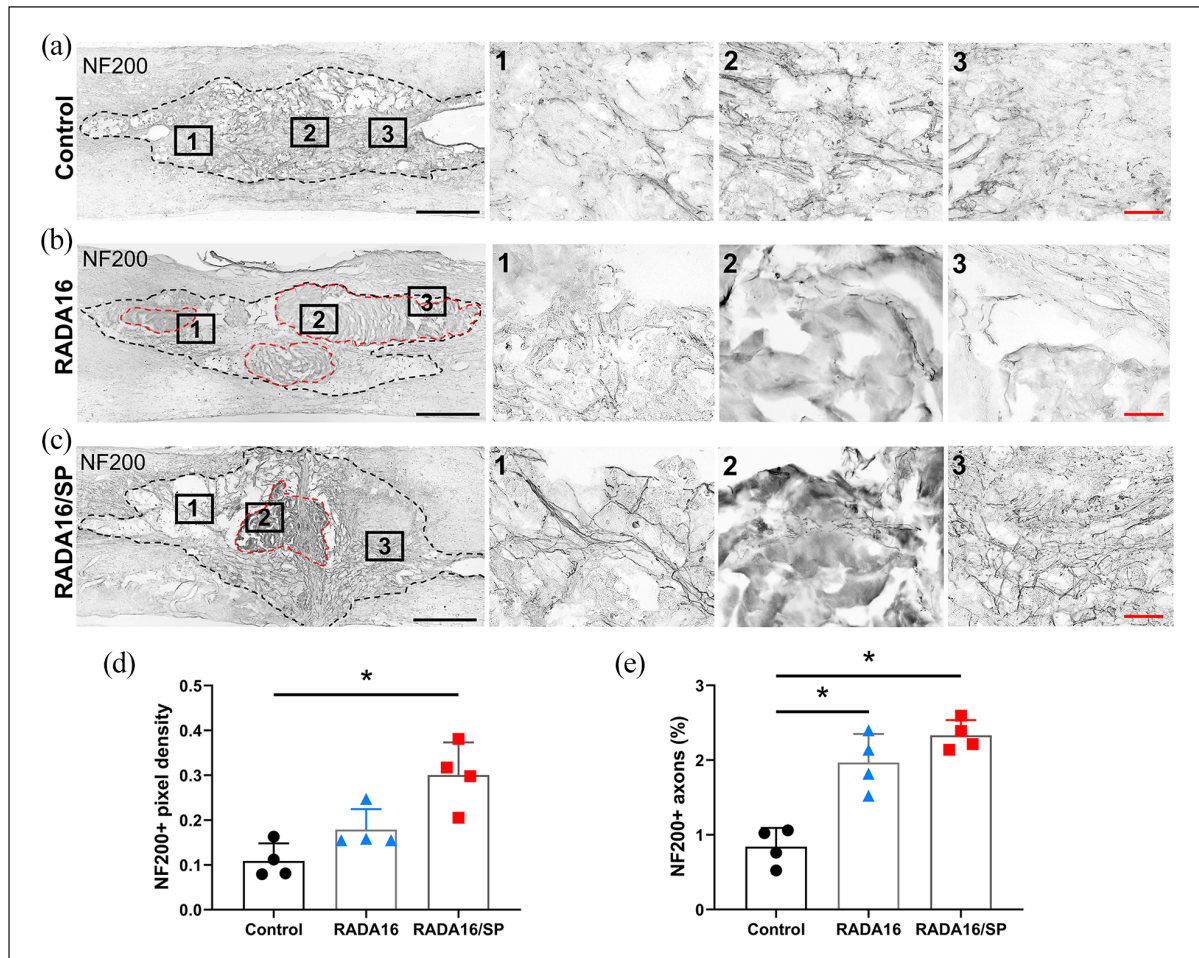


Figure 5. Representative NF200- and DAB-stained images of sagittal spinal cord sections from the control (a), RADA16 (b) and RADA16/SP (c) groups 8 weeks after injection within the lesion cavities of contused spinal cords (outlined by black dashed lines). Injected hydrogels are remained within the lesion cavity in RADA16 and RADA16/SP groups (outlined by red dashed lines). A 10 \times objective was used to obtain these images; black scale bar, 500 μ m. The black boxes are magnified on the right side; red scale bar, 50 μ m. The mean density (d) and percentage of NF200+ axons within the lesion epicenter (e) were quantified in 3 20 \times fields ($n=4$ per group). * $p < 0.05$, one-way ANOVA followed by the Games-Howell post hoc test.

and microglia were not changed when only RADA16 was applied (Figure 3).

The cavity size was not changed in the RADA16 or RADA16 + RADA16-SP group compared to the control group (Figure 3). The lesion cavity is surrounded by glial scar tissue, which is activated by inflammatory cytokines (e.g. IL-6 and IL-1 β) secreted by resident and infiltrating inflammatory cells.^{1,27} In this study, we found the levels of that pro-inflammatory genes, including IL-6, IL-1 β , and caspase 3, were not changed in the RADA16/SP group compared to the control group. Therefore, the lack of difference in the size of the lesion cavity between the RADA16/SP group and the control group might have been related to the lack of change in the expression of pro-inflammatory cytokines.

In a previous study in which the combination of RADA16 and neural stem/progenitor cells was applied to the contused spinal cords of rats, the application of RADA16 without cells was found to also induce decreases

in the lesion volume and functional recovery.¹⁴ However, the amount of RADA16 hydrogel applied in their study was 10 times higher than that applied in our study (100 vs 10 μ L, respectively), and no molecular analysis was performed. In another study, a mixture of RADA16 and SVVYGLR derived from osteopontin was applied to brain injury model zebrafish, but no functional recovery was observed after RADA16 application.¹⁵ Therefore, the role of RADA16 in neuronal regeneration in the CNS might be supportive, and the main effects of RADA16-based hydrogels might be determined by the added biomaterials or cells.

The mixture of RADA16 and RADA16-SP promoted an increase in CD31+ and VEGF+ vessel formation and NF200+ axon regeneration within the lesion cavity (Figures 4 and 5). Moreover, all of these changes facilitated functional recovery in SCI rat models (Figure 7). Substance P is released from sensory neurons after

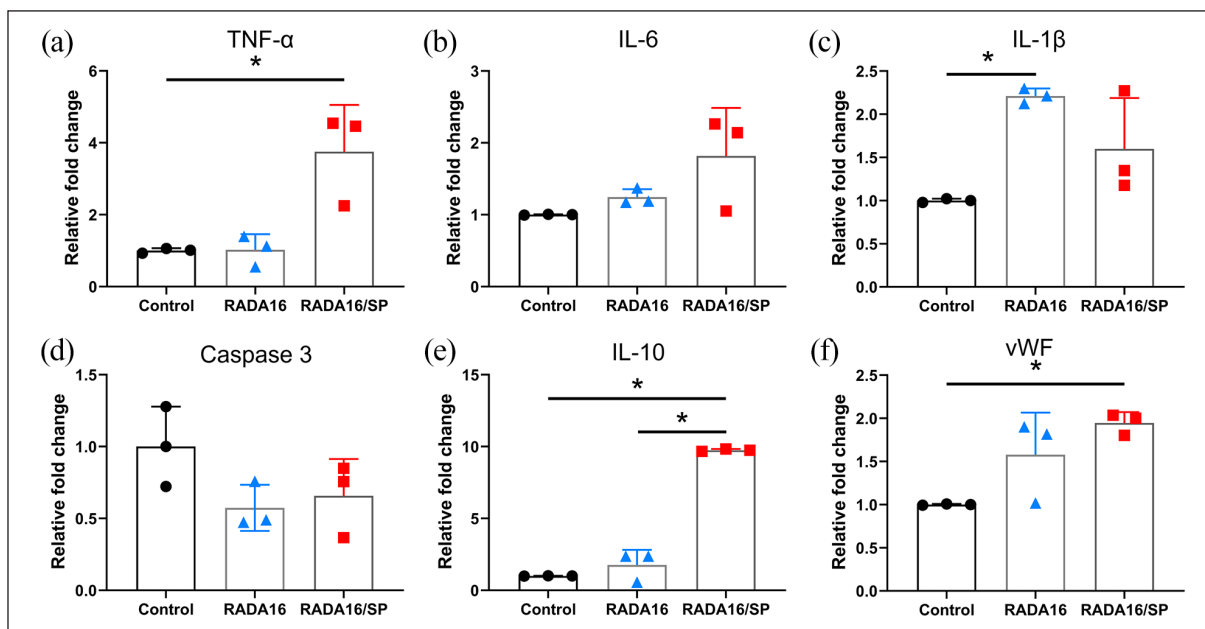


Figure 6. The relative mRNA expression levels of genes associated with inflammation and angiogenesis in the control, RADA16 and RADA16/SP groups 8 weeks after injection ($n=3$ per group). (a) TNF- α , (b) IL-6, (c) IL-1 β , (d) caspase 3, (e) IL-10, and (f) vWF levels. * $p < 0.05$, one-way ANOVA followed by the Games-Howell post hoc test.

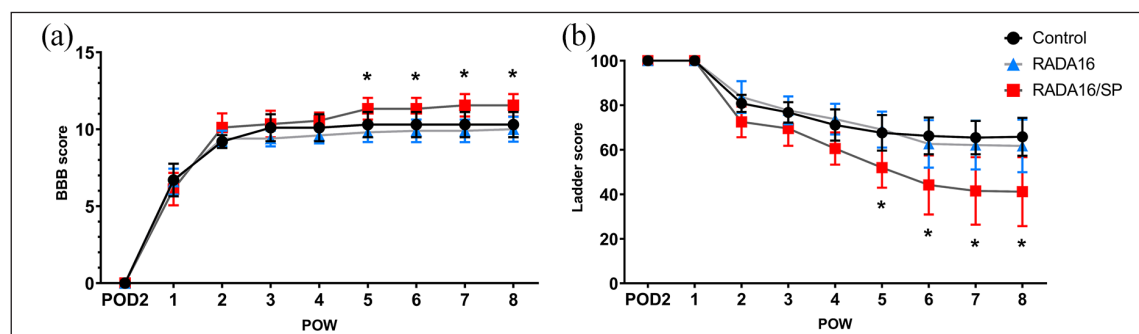


Figure 7. The hindlimb movement of the control, RADA16 and RADA16/SP groups was assessed with the BBB scale (a) and horizontal ladder test (b) over an 8-week period postinjury ($n=10$ in the control and RADA16 groups, $n=9$ in the RADA16/SP group). The data are expressed as the mean \pm SD. * $p < 0.05$ between the control and RADA16/SP groups, two-way ANOVA followed by the Bonferroni post hoc test.

damage, binds and activates the neurokinin 1 receptor and induces inflammation, angiogenesis, tissue homeostasis, and wound healing.^{16,28} Various hydrogels containing anionic gelatin,¹⁸ chitosan hydrochloride,²⁹ or laponite nanodiscs³⁰ have been used to induce sustained and controlled release of substance P, and these hydrogels have been found to successfully support the main functions of substance P in the skin and subcutaneous layer. In this study, RADA16 gradually secreting substance P in the injured spinal cord, as in a previous study on limb ischemia.²⁰

We found that TNF- α gene expression was increased in the RADA16/SP group compared with the control and RADA16 groups (Figure 6(a)) and that the expression levels of the inflammatory cytokines, IL-6, IL-1 β , and

caspase 3 were not different between the RADA16/SP and control groups (Figure 6(b)–(d)). Some previous studies have revealed that the suppression of TNF- α modulates inflammation and enhances functional recovery after SCI,^{31,32} whereas TNF- α promotes axonal regeneration in the spinal cord³³ and angiogenesis in bone and dental pulp.^{34,35} Other studies have reported the different roles of TNF- α and IL-1 β in CNS lesions. While TNF- α promotes axonal regeneration or mediates neuroprotection in CNS lesions, IL-1 β does not show these effects.^{33,36} In addition, TNF- α has been shown to exert a potent anti-inflammatory effect in previous studies.^{37,38} Previous studies have reported that endogenous substance P binds to neurokinin type 1 receptor and increases TNF- α gene expression.^{39,40}

In this study, upregulation of TNF- α gene expression due to the sustained release of exogenous substance P up to 8 weeks after SCI might have affected functional improvement, and direct or indirect anti-inflammatory reactions might have reduced the numbers of macrophages and microglia after SCI; however, further study is needed to confirm these speculations.

In this study, IL-10 gene expression was significantly increased in the RADA16/SP group (Figure 6(e)). In previous studies, sustained delivery of exogenous IL-10 was shown to be effective in improving functional recovery in rodent SCI models.^{41,42} IL-10 is a major anti-inflammatory cytokine that mediates macrophage polarization toward the M2 phenotype.⁴³ Substance P also induces M2 macrophage polarization and leads to functional improvement in rat models of spinal cord contusion injury.^{44,45} Although we did not evaluate the distribution of M1 and M2 macrophages in the present study, M2 macrophage polarization is closely related to functional recovery in SCI models, as found in our previous study.²² Therefore, M2 polarization induced by substance P might affect functional recovery in SCI models.

The expression of vWF was upregulated in the RADA16/SP group (Figure 6(f)). vWF regulates blood vessel formation by modulating VEGF receptor signaling and enhancing vessel maturation,⁴⁶ and clinically, vWF dysfunction causes vascular malformation and a bleeding tendency.⁴⁷ The increase in the mRNA level of vWF is in good agreement with the increase in the number of blood vessels shown in Figure 4, and increased vWF mRNA expression can explain the effect of RADA16 modified with substance P after SCI.

Prominent functional improvements were observed in the RADA16/SP group from 5 weeks after injection until sacrifice (Figure 7(a) and (b)). In this study, the mixture of RADA16 and RADA16-SP successfully promoted axonal sprouting within the lesion cavity and increased angiogenesis, and these changes might have contributed to the promotion of functional recovery. Previous studies using poly(lactic-co-glycolic acid) (PLGA) microspheres containing VEGF and basic fibroblast growth factors⁴ or direct application of VEGF⁴⁸ showed good functional improvement, whereas other studies using graphene oxide scaffolds⁴⁹ or reduced graphene oxide sheets,⁵⁰ which also promote angiogenesis after SCI, did not show any functional improvement. The use of growth factors in the clinical field is strictly limited, and only a small number of growth factors, such as platelet-derived growth factor and bone morphogenic proteins, have been approved by the US Food and Drug Administration (FDA).^{51,52} RADA16 is already used in the clinical setting as a hemostatic agent, and another self-assembling peptide, EAK16, is also used for wound healing and tissue regeneration.^{12,25} Therefore, RADA16 and modified versions of RADA16 might be approved for clinical application faster than VEGF or angiogenesis-related growth factors.

Peptide-based functional hydrogels are used to construct in vitro 3D culture systems for cancer research.^{53,54}

In order for hydrogels to be useful for constructing in vitro 3D culture systems in various fields, their stiffness, adhesion properties, and porosity need to be controllable to allow the growth and interactions of various types of cells.^{55,56} The stiffness of RADA16 can be sufficiently modified by the addition functional groups, which might be useful for the development of ideal 3D culture systems for the field of tissue regeneration.

In this study, we did not examine the molecular changes in the damaged spinal cord at the acute and subacute stages, which might be helpful for determining the effects of RADA modified with substance P on the initial inflammatory process, and substance P-induced macrophage polarization also needs to be evaluated in future studies to confirm its contribution to functional improvement.

Conclusions

Herein, we concluded that the self-assembling peptide RADA16 modified with substance P enhances functional improvement in a rat model of spinal cord contusion injury and that angiogenesis might be an important factor in promoting neuronal regeneration following SCI.

Declaration of conflicting interests


The author(s) declared no potential conflicts of interest with respect to the research, authorship, and/or publication of this article.

Funding

The author(s) disclosed receipt of the following financial support for the research, authorship, and/or publication of this article: This work was supported by the National Research Foundation (NRF) and the Ministry of Science and ICT (MSIT) (2019R1A6A1A11034536, 2020R1A2C2004764); the Korea Medical Device Development Fund grant funded by the Korean government (the Ministry of Science and ICT; the Ministry of Trade, Industry and Energy (MOTIE); the Ministry of Health & Welfare; the Ministry of Food and Drug Safety) (202017D01); the MOTIE (20008686); and the KU-KIST Graduate School of Converging Science and Technology Program, Republic of Korea.

ORCID iDs

Jooik Jeon  <https://orcid.org/0000-0001-5781-7706>

Jung Keun Hyun  <https://orcid.org/0000-0001-9254-4424>

References

1. Alizadeh A, Dyck SM and Karimi-Abdolrezaee S. Traumatic Spinal cord Injury: an overview of pathophysiology, models and acute injury mechanisms. *Front Neurol* 2019; 10: 282.
2. Hyun JK and Kim HW. Clinical and experimental advances in regeneration of spinal cord injury. *J Tissue Eng* 2010; 2010: 650857.
3. Kundi S, Bicknell R and Ahmed Z. The role of angiogenic and wound-healing factors after spinal cord injury in mammals. *Neurosci Res* 2013; 76: 1–9.

4. Yu S, Yao S, Wen Y, et al. Angiogenic microspheres promote neural regeneration and motor function recovery after spinal cord injury in rats. *Sci Rep* 2016; 6: 33428.
5. Rocha LA, Sousa RA, Learmonth DA, et al. The role of biomaterials as angiogenic modulators of spinal cord injury: mimetics of the spinal cord, cell and angiogenic factor delivery agents. *Front Pharmacol* 2018; 9: 164.
6. Dashnyam K, El-Fiqi A, Buitrago JO, et al. A mini review focused on the proangiogenic role of silicate ions released from silicon-containing biomaterials. *J Tissue Eng* 2017; 8: 2041731417707339.
7. Menezes K, Rosa BG, Freitas C, et al. Human mesenchymal stromal/stem cells recruit resident pericytes and induce blood vessels maturation to repair experimental spinal cord injury in rats. *Sci Rep* 2020; 10: 19604.
8. Zhong D, Cao Y, Li CJ, et al. Neural stem cell-derived exosomes facilitate spinal cord functional recovery after injury by promoting angiogenesis. *Exp Biol Med* 2020; 245: 54–65.
9. Cao Y, Xu Y, Chen C, et al. Local delivery of USC-derived exosomes harboring ANGPTL3 enhances spinal cord functional recovery after injury by promoting angiogenesis. *Stem Cell Res Ther* 2021; 12: 20.
10. Yahata K, Kanno H, Ozawa H, et al. Low-energy extracorporeal shock wave therapy for promotion of vascular endothelial growth factor expression and angiogenesis and improvement of locomotor and sensory functions after spinal cord injury. *J Neurosurg Spine* 2016; 25: 745–755.
11. Yokoi H, Kinoshita T and Zhang S. Dynamic reassembly of peptide RADA16 nanofiber scaffold. *Proc Natl Acad Sci USA* 2005; 102: 8414–8419.
12. Sankar S, O'Neill K, Bagot D'Arc M, et al. Clinical use of the self-assembling peptide RADA16: a review of current and future trends in biomedicine. *Front Bioeng Biotechnol* 2021; 9: 679525.
13. Tran KA, Partyka PP, Jin Y, et al. Vascularization of self-assembled peptide scaffolds for spinal cord injury repair. *Acta Biomater* 2020; 104: 76–84.
14. Abdolahi S, Aligholi H, Khodakaram-Tafti A, et al. Improvement of rat spinal cord injury following lentiviral vector-transduced neural stem/progenitor cells derived from human epileptic brain tissue transplantation with a self-assembling peptide scaffold. *Mol Neurobiol* 2021; 58: 2481–2493.
15. Wang TW, Chang KC, Chen LH, et al. Effects of an injectable functionalized self-assembling nanopeptide hydrogel on angiogenesis and neurogenesis for regeneration of the central nervous system. *Nanoscale* 2017; 9: 16281–16292.
16. Amadesi S, Reni C, Katare R, et al. Role for substance p-based nociceptive signaling in progenitor cell activation and angiogenesis during ischemia in mice and in human subjects. *Circulation* 2012; 125: 1774–1786.
17. Im H, Kim SH, Kim SH, et al. Skin regeneration with a scaffold of predefined shape and bioactive peptide hydrogels. *Tissue Eng Part A* 2018; 24: 1518–1530.
18. Kohara H, Tajima S, Yamamoto M, et al. Angiogenesis induced by controlled release of neuropeptide substance P. *Biomaterials* 2010; 31: 8617–8625.
19. Dzurik MV, Diedrich A, Black B, et al. Endogenous substance P modulates human cardiovascular regulation at rest and during orthostatic load. *J Appl Physiol* 2007; 102: 2092–2097.
20. Kim JH, Jung Y, Kim BS, et al. Stem cell recruitment and angiogenesis of neuropeptide substance P coupled with self-assembling peptide nanofiber in a mouse hind limb ischemia model. *Biomaterials* 2013; 34: 1657–1668.
21. Kim JE, Lee JH, Kim SH, et al. Skin regeneration with self-assembled peptide hydrogels conjugated with substance P in a diabetic rat model. *Tissue Eng Part A* 2018; 24: 21–33.
22. Hong JY, Seo Y, Davaa G, et al. Decellularized brain matrix enhances macrophage polarization and functional improvements in rat spinal cord injury. *Acta Biomater* 2020; 101: 357–371.
23. Kim SH, Hur W, Kim JE, et al. Self-assembling peptide nanofibers coupled with neuropeptide substance P for bone tissue engineering. *Tissue Eng Part A* 2015; 21: 1237–1246.
24. Basso DM, Beattie MS and Bresnahan JC. Graded histological and locomotor outcomes after spinal cord contusion using the NYU weight-drop device versus transection. *Exp Neurol* 1996; 139: 244–256.
25. Gelain F, Luo Z, Rioult M, et al. Self-assembling peptide scaffolds in the clinic. *NPJ Regen Med* 2021; 6: 9.
26. Zhang S. Discovery and design of self-assembling peptides. *Interface Focus* 2017; 7: 20170028.
27. Orr MB and Gensel JC. Spinal cord injury scarring and inflammation: therapies targeting glial and inflammatory responses. *Neurother* 2018; 15: 541–553.
28. Suvas S. Role of substance P neuropeptide in inflammation, wound healing, and tissue homeostasis. *J Immunol* 2017; 199: 1543–1552.
29. Li H, Li M, Liu P, et al. A multifunctional substance P-conjugated chitosan hydrochloride hydrogel accelerates full-thickness wound healing by enhancing synchronized vascularization, extracellular matrix deposition, and nerve regeneration. *Biomater Sci* 2021; 9: 4199–4210.
30. De Serres-Bérard T, Becher TB, Braga CB, et al. Neuropeptide Substance P released from a nonswellable laponite-based hydrogel enhances wound healing in a tissue-engineered skin in vitro. *ACS Appl Polym Mater* 2020; 2: 5790–5797.
31. Huang JH, Yin XM, Xu Y, et al. Systemic administration of exosomes released from mesenchymal stromal cells attenuates apoptosis, inflammation, and promotes angiogenesis after spinal cord injury in rats. *J Neurotrauma* 2017; 34: 3388–3396.
32. Zhang X, Shi LL, Gao X, et al. Lentivirus-mediated inhibition of tumour necrosis factor- α improves motor function associated with PRDX6 in spinal cord contusion rats. *Sci Rep* 2015; 5: 8486.
33. Tsarouchas TM, Wehner D, Cavone L, et al. Dynamic control of proinflammatory cytokines Il-1 β and Tnf- α by macrophages in zebrafish spinal cord regeneration. *Nat Commun* 2018; 9: 4670.
34. Wang Y, Xu J, Zhang X, et al. TNF- α -induced LRG1 promotes angiogenesis and mesenchymal stem cell migration in the subchondral bone during osteoarthritis. *Cell Death Discov* 2017; 8: e2715.
35. Shin MR, Kang SK, Kim YS, et al. TNF- α and LPS activate angiogenesis via VEGF and SIRT1 signalling in human dental pulp cells. *Int Endod J* 2015; 48: 705–716.
36. Turrin NP and Rivest S. Tumor necrosis factor alpha but not interleukin 1 beta mediates neuroprotection in response to acute nitric oxide excitotoxicity. *J Neurosci* 2006; 26: 143–151.

37. Masli S and Turpie B. Anti-inflammatory effects of tumour necrosis factor (TNF)-alpha are mediated via TNF-R2 (p75) in tolerogenic transforming growth factor-beta-treated antigen-presenting cells. *Immunology* 2009; 127: 62–72.
38. Zakharova M and Ziegler HK. Paradoxical anti-inflammatory actions of TNF-alpha: inhibition of IL-12 and IL-23 via TNF receptor 1 in macrophages and dendritic cells. *J Immunol* 2005; 175: 5024–5033.
39. Wang H, Zhang X, He JY, et al. Increasing expression of substance P and calcitonin gene-related peptide in synovial tissue and fluid contribute to the progress of arthritis in developmental dysplasia of the hip. *Arthritis Res Ther* 2015; 17: 4.
40. Gautam M, Prasoon P, Kumar R, et al. Role of neurokinin type 1 receptor in nociception at the periphery and the spinal level in the rat. *Spinal Cord* 2016; 54: 172–182.
41. Hellenbrand DJ, Reichl KA, Travis BJ, et al. Sustained interleukin-10 delivery reduces inflammation and improves motor function after spinal cord injury. *J Neuroinflammation* 2019; 16: 93.
42. Ciciriello AJ, Smith DR, Munsell MK, et al. IL-10 lentivirus-laden hydrogel tubes increase spinal progenitor survival and neuronal differentiation after spinal cord injury. *Biotechnol Bioeng* 2021; 118: 2609–2625.
43. Lopes RL, Borges TJ, Zanin RF, et al. IL-10 is required for polarization of macrophages to m2-like phenotype by mycobacterial DnaK (heat shock protein 70). *Cytokine* 2016; 85: 123–129.
44. Lim JE, Chung E and Son Y. A neuropeptide, Substance-P, directly induces tissue-repairing M2 like macrophages by activating the PI3K/Akt/mTOR pathway even in the presence of IFN γ . *Sci Rep* 2017; 7: 9417.
45. Jiang MH, Chung E, Chi GF, et al. Substance P induces m2-type macrophages after spinal cord injury. *Neuroreport* 2012; 23: 786–792.
46. Randi AM and Laffan MA. Von Willebrand factor and angiogenesis: basic and applied issues. *J Thromb Haemost* 2017; 15: 13–20.
47. Randi AM, Smith KE and Castaman G. von Willebrand factor regulation of blood vessel formation. *Blood* 2018; 132: 132–140.
48. Widenfalk J, Lipson A, Jubran M, et al. Vascular endothelial growth factor improves functional outcome and decreases secondary degeneration in experimental spinal cord contusion injury. *Neuroscience* 2003; 120: 951–960.
49. López-Dolado E, González-Mayorga A, Gutiérrez MC, et al. Immunomodulatory and angiogenic responses induced by graphene oxide scaffolds in chronic spinal hemisectioned rats. *Biomaterials* 2016; 99: 72–81.
50. Domínguez-Bajo A, González-Mayorga A, Guerrero CR, et al. Myelinated axons and functional blood vessels populate mechanically compliant rGO foams in chronic cervical hemisectioned rats. *Biomaterials* 2019; 192: 461–474.
51. Yamakawa S and Hayashida K. Advances in surgical applications of growth factors for wound healing. *Burns Trauma* 2019; 7: 10.
52. Spiller KL and Vunjak-Novakovic G. Clinical translation of controlled protein delivery systems for tissue engineering. *Drug Deliv Transl Res* 2015; 5: 101–115.
53. Worthington P, Pochan DJ and Langhans SA. Peptide hydrogels – versatile matrices for 3D cell culture in cancer medicine. *Front Oncol* 2015; 5: 92.
54. Xu J, Qi G, Wang W, et al. Advances in 3D peptide hydrogel models in cancer research. *NPJ Sci Food* 2021; 5: 14.
55. Sällström N, Capel A, Lewis MP, et al. 3D-printable zwitterionic nano-composite hydrogel system for biomedical applications. *J Tissue Eng* 2020; 11: 2041731420967294.
56. Tunesi M, Izzo L, Raimondi I, et al. A miniaturized hydrogel-based in vitro model for dynamic culturing of human cells overexpressing beta-amyloid precursor protein. *J Tissue Eng* 2020; 11: 2041731420945633.